Interband transitions and phonon modes in $B_xGa_{1-x}As$ ($0 \leqslant x \leqslant 0.03$) and GaN_yAs_{1-y} ($0 \leqslant y \leqslant 0.037$): A comparison

Gunnar Leibiger* and Volker Gottschalch
Fakultät für Chemie und Mineralogie, Universität Leipzig, Linnéstraße 3, 04103 Leipzig, Germany

Volker Riede and Mathias Schubert
Fakultät für Physik und Geowissenschaften, Universität Leipzig, Linnéstraße 5, 04103 Leipzig, Germany

James N. Hilfiker and Thomas E. Tiwald
John A. Woollam Company, Incorporated, 645 M Street, Lincoln, Nebraska 68508

(Received 30 July 2002; revised manuscript received 28 October 2002; published 22 May 2003)

We report on the experimental observation of direct interband-critical-point transitions and phonon modes in $B_xGa_{1-x}As$ alloys ($0 \leqslant x \leqslant 0.03$) and their evolution with increasing boron concentration using spectroscopic ellipsometry and Raman scattering. Our results are compared to the corresponding values in the GaN_yAs_{1-y} ($0 \leqslant y \leqslant 0.037$) material system. For $B_xGa_{1-x}As$, we obtain only a small bowing coefficient of the $E_g(x)$ dependence in contrast to the giant redshift of the GaN_yAs_{1-y} band-gap energy with y. The higher lying interband-transition energies of $B_xGa_{1-x}As$ (E_1,$E_1+\Delta_1$, E_0', E_2, and E_1') are slightly redshifted with increasing boron concentration. A similar behavior is found for the critical points $E_0{}'$, E_2, and $E_1{}'$ in GaN_yAs_{1-y}. In $B_xGa_{1-x}As$, we observe, as in GaN_yAs_{1-y}, a two-mode phonon behavior using Raman scattering. However, from infrared-ellipsometry or -transmission experiments, we can estimate that the oscillator strength or polarity of the BAs-like phonon is at least one order of magnitude smaller than the oscillator strength of the GaN-like phonon measured at a GaN_yAs_{1-y} layer with comparable thickness and composition. All results will be explained using a simple model that takes into account the different nature of the chemical bonds in both alloy types.

DOI: 10.1103/PhysRevB.67.195205 PACS number(s): 71.20.−b, 71.22.+i, 71.70.−d, 78.20.−e

I. INTRODUCTION

GaN_yAs_{1-y} alloys have attracted wide interest in the past few years due to their interesting electronic properties and possible device applications, e.g., for 1.3–1.55-μm laser diodes (for a review, see for instance Ref. 1).[2,3] $B_xGa_{1-x}As$ is a novel material system of fundamental interest, which offers new possibilities in semiconductor-band-gap engineering and, in addition, for optoelectronic devices, such as solar cells.[4,5] $B_xGa_{1-x}As$ ternary compounds result from alloying of the binary compounds GaAs ($a_0=5.6533$ Å) and cubic BAs ($a_0=4.777$ Å),[6] leading to a lattice mismatch of 16% for $x=1$. Thus, incorporation of the small B atom in $In_zGa_{1-z}As$ alloys with $z=2.2x$, and assuming Vegard's law, results in quaternary layers that are lattice matched to GaAs. This property makes $B_xGa_{1-x-z}In_zAs$ alloys very interesting for application in detector structures and solar cells. For cubic BAs, theoretical studies predict values for the indirect band-gap energy ranging from 1.27 to 1.86 eV,[5,7] and for the direct band-gap energy from 3.05 to 4.23 eV (Refs. 5 and 8) (an experimental band-gap energy of 1.46 eV has been reported in Refs. 9 and 10 for polycrystalline BAs; it is not clear whether this band gap is direct or indirect). For $B_xGa_{1-x}As$ alloys ($0 \leqslant x \leqslant 4\%$), a small increase of the band-gap energy with increasing boron incorporation has already been reported.[4,5,11–13] The corresponding bowing parameters varied between 1.6 (Ref. 13) and 3.5 eV.[5] These values are in strong contrast to the GaN_yAs_{1-y} alloy system, for which a large and composition-dependent bowing parameter was obtained.[2,14] The fundamental difference between the alloys $B_xGa_{1-x}As$ and GaN_yAs_{1-y} is the nature of their chemical bonds. The B-As and Ga-N bonds differ strongly in their ionicity values, which, as will be shown below, causes fundamental differences in the electronic and vibronic properties of both alloy types.

In early reports, boron doping in (Al,Ga)As was investigated including MOVPE (metal-organic vapor-phase epitaxy) and MBE (molecular beam cpitaxy) growth data, electrical and morphologic properties.[15,16] Geisz *et al.* reported on the MOVPE growth of (B,Ga,In)As alloys with boron concentrations up to 4%.[4,11] The authors report on a slight increase of the band-gap energy of $B_xGa_{1-x}As$ with increasing boron incorporation, and a bowing parameter of 2 eV.[4] This was confirmed by photoluminescence (PL) measurements presented in Ref. 12 for boron concentrations up to 1%. Hart and Zunger presented a theoretical study of the electronic structure of BAs and boron containing III-V ternary alloys.[5] For the $B_xGa_{1-x}As$ alloys, the authors predict a relatively small and composition independent band-gap bowing. In Ref. 13, we reported on the MOVPE growth of BGaAs, BAlAs, BAlGaAs, and BGaInAs alloys. We demonstrated room-temperature photoluminescence of $B_xGa_{1-x}As$ ($0 \leqslant x \leqslant 0.032$) and $B_xGa_{1-x-z}In_zAs$ lattice matched to GaAs (several compositions, E_{gap} down to 1.36 eV). $B_xGa_{1-x}As$/GaAs and $B_xGa_{1-x-z}In_zAs$/GaAs multiple quantum well structures with high structural quality have been achieved.[13] A study of $B_xGa_{1-x-z}In_zAs$ as active material in laser diodes will be published elsewhere.

In the present work we want to address the following issues: (1) the evolution of several direct critical-point (CP) transitions within the Brillouin zone (BZ) of $B_xGa_{1-x}As$ ($0 \leqslant x \leqslant 0.03$) with increasing boron incorporation; (2) the phonon mode behavior of $B_xGa_{1-x}As$ ($0 \leqslant x \leqslant 0.03$); (3) a comparison between these properties and those of the GaN_yAs_{1-y} alloy system, and we will provide a simple explanation for the observed differences. Properties of electronic interband transitions and phonon modes are obtained using spectroscopic ellipsometry (SE) for photon energies from 0.75 to 8 eV and for wave numbers from 150 to 600 cm^{-1} upon model line-shape analysis of the dielectric function of $B_xGa_{1-x}As$ and GaN_yAs_{1-y} alloys. Additionally, we use Raman scattering for analyzing the phonon properties of the $B_xGa_{1-x}As$ compounds. The SE investigations for wave numbers from 100 to 600 cm^{-1} and for photon energies from 0.75 to 4.5 eV of GaN_yAs_{1-y} single layers (using the same samples as in the present work) and superlattice structures have already been presented in Refs. 17,18 and 19,20, respectively.

II. EXPERIMENT AND DATA ANALYSIS

The $B_xGa_{1-x}As$ layers (thickness $\sim$400 nm) were grown pseudomorphically on (001) GaAs substrates at growth temperatures ranging between 550 °C and 600 °C using low-pressure ($p_{tot}=50$ mbar) metal-organic vapor-phase epitaxy (MOVPE). Triethylboron, trimethylgallium, and arsine were used as precursors. A GaAs buffer layer of about 150 nm thickness was deposited prior to the $B_xGa_{1-x}As$ layer. The B concentration was determined by high-resolution x-ray diffraction. For details of the MOVPE growth, we refer to Ref. 13. MOVPE-growth properties of our GaN_yAs_{1-y}/GaAs samples are included in Refs. 17 and 18.

The SE spectra were recorded at room temperature at 75° and 50° angle of incidence for photon energies from 0.75 to 8 eV in steps of 10 meV (2 meV for the low-energy part) and for wave numbers from 150 to 600 cm^{-1} with 2 cm^{-1}, respectively. A variable-angle-of-incidence, rotating-analyzer spectroscopic ellipsometer equipped with an automated retarder, was utilized. Ellipsometry can determine the complex dielectric function ϵ and thickness d of a thin-film sample by comparing the measured data with the best-fit model calculations. In the photon-energy range of direct electronic band-to-band transitions, which cause typical CP structures in ϵ, CP energies, amplitudes, and broadening parameters can be obtained as best-fit parameters from model analysis of ellipsometric spectra. The standard ellipsometric quantities Ψ and Δ are related to the complex reflectance ratio ρ[21]

$$\rho \equiv r_p / r_s = \tan\Psi \exp i\Delta, \tag{1}$$

where r_p and r_s are the reflection coefficients for light polarized parallel (p), and perpendicular (s) to the plane of incidence, respectively. The pseudodielectric function $\langle\varepsilon\rangle$ is a common representation of the ellipsometric data Ψ and Δ[22]

$$\langle\varepsilon\rangle \equiv \varepsilon_a\{[(1-\rho)/(1+\rho)]^2 \sin^2\Phi_a + \cos^2\Phi_a\}\tan^2\Phi_a . \tag{2}$$

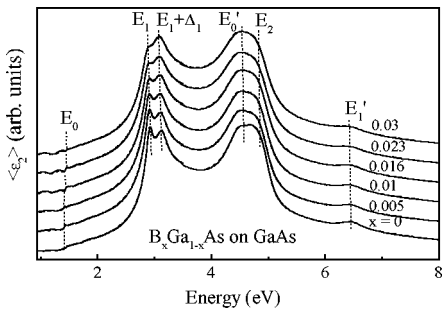

FIG. 1. Imaginary part of the pseudodielectric function of the $B_xGa_{1-x}As$/GaAs samples. The dashed and solid lines refer to the experimental and best-fit calculated spectra, respectively. The spectra of the samples with $x \geqslant 0.005$ have been shifted for better clarity.

For description of the dielectric function of our $B_xGa_{1-x}As$ and GaN_yAs_{1-y} layers, we used a composite model dielectric function (MDF), which consists of contributions of the following direct CP transitions to ϵ: $E_0, E_0+\Delta_0, E_1, E_1+\Delta_1, E_0', E_2$, and E_1'. The expressions for the CP's E_0, $E_0+\Delta_0$, E_1, and $E_1+\Delta_1$ can be found in Refs. 23 and 24. The contributions of the three CP transitions with transition energies higher than that of $E_1+\Delta_1$ to ϵ are described by Lorentzian functions. For a more detailed description of the ellipsometric model analysis and the applied MDF's, we refer to Refs. 18 and 25, where we reported on critical points, optical constants, and phonon properties of III-V alloys studied by SE.

The Raman spectra were recorded at room temperature using a Dilor XY800 spectrometer in macromode position with 2 cm^{-1} resolution. The 514.5-nm line of an Ar-ion laser with a laser power of 50 mW was used as excitation source. All spectra were recorded in the backscattering configuration.

III. RESULTS AND DISCUSSION

A. Direct interband transitions

In Fig. 1, we present the imaginary part of the pseudodielectric function of our $B_xGa_{1-x}As$/GaAs samples. The dashed lines are the experimental spectra, whereas the solid lines refer to the best-fit model calculation using the MDF described above. Note that solid and dashed lines in Fig. 1 are almost undistinguishable due to the good match between experimental and best-fit calculated data. Note further that the spectra from 0.75 to 3.5 eV and from 3.5 to 8 eV have been measured at different times, which explains the small offset in the spectra at an energy of 3.5 eV. However, except for a different oxide-layer thickness to account for the natural oxide which develops on the surface during the course of our experiments, we used exactly the same MDF with the same MDF parameters for modeling the pseudodielectric-function spectra in both energy ranges. The vertical dotted lines mark the energies of the CP's E_0, E_1, $E_1+\Delta_1$, E_0', E_2, and E_1' resulting from the best-fit analysis. Note that these assignments of CP structures have originally been made for GaAs.[26–28] In the present work, we adopt these

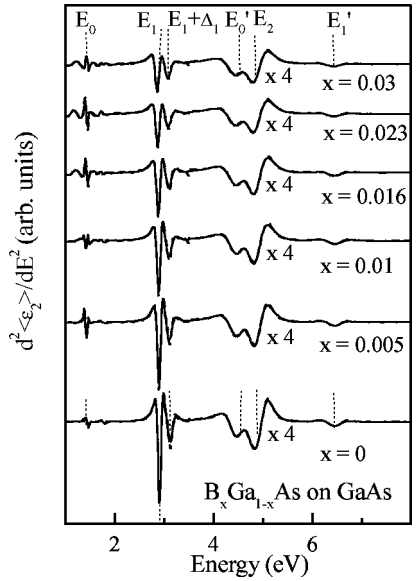

FIG. 2. Second derivative of the imaginary part of the pseudodielectric function of the $B_xGa_{1-x}As/GaAs$ samples. The dashed and solid lines refer to the experimental and best-fit calculated spectra, respectively. The spectra of the samples with $x \geqslant 0.005$ have been shifted for better clarity. The high-energy part (3.5–8 eV) of all spectra has been magnified by a factor of 4.

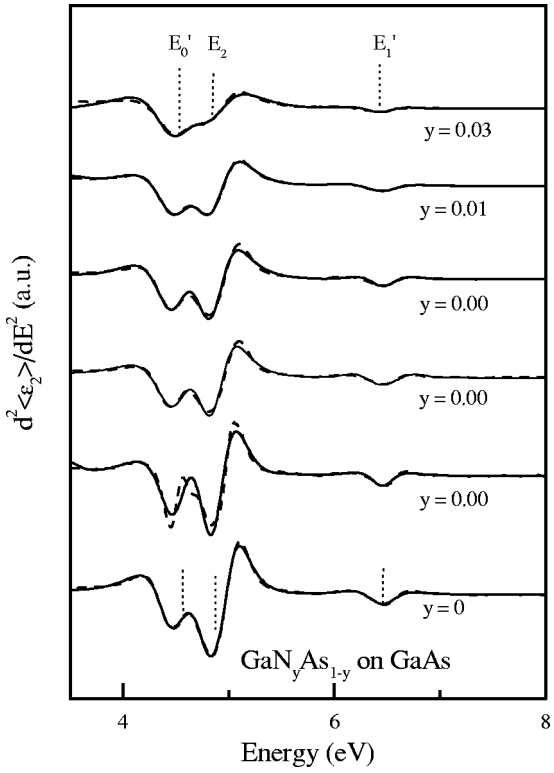

FIG. 3. Second derivative of the imaginary part of the pseudodielectric function of the GaN_yAs_{1-y}/GaAs samples. The dashed and solid lines refer to the experimental and best-fit calculated spectra. The spectra of the samples with $y \geqslant 0.001$ have been shifted for better clarity.

assignments to the $B_xGa_{1-x}As$ alloys, thereby starting from a GaAs reference sample, which is also included in Fig. 1. The different CP transitions will be explained in the following.

The dominant structure at about 3 eV is due to the CP's E_1 and $E_1+\Delta_1$. These M_1-type critical points are due to electronic interband transitions occuring along the Λ direction of the BZ.[26] We note a slight increase of the broadening of the E_1 and $E_1+\Delta_1$ transitions with increasing boron incorporation in Fig. 1, which we attribute to compositional fluctuations. The small features labeled E_0 at about 1.4 eV are due the direct band-gap transitions. Distinct oscillations occur for photon energies below E_0, except for the GaAs reference sample ($x=0$). These oscillations are due to multiple reflections at the sample surface and the $B_xGa_{1-x}As/GaAs$ interface leading to well-known optical interference pattern. The other dominant structure at about 5 eV can be well described by two distinct transitions that we assign to the CP's $E_0{}'$ and E_2. The two CP's are due to direct transitions at the center of the BZ ($E_0{}'$) and around the x point (E_2).[27,28] Note, however, that in the spectral region from 4.5 to 5.2 eV there is an accumulation of several CP's in GaAs (except from various transitions at the center of the BZ and around the x point, there are further transitions along the Δ and Σ lines), which makes the unambiguous assignment of these structures difficult.[26–28] The weak structure at about 6.5 eV labeled $E_1{}'$ is due to transitions either along the Λ direction or at the L point of the BZ.[26,27]

In Fig. 2, we show the second derivatives of the imaginary parts of the pseudodielectric functions of the $B_xGa_{1-x}As$ samples. Derivative spectra are shown because all CP transitions are more pronounced than in the undifferentiated pseudodielectric-function spectra (Fig. 1). Note that we have not explicitly included the derivative spectra into the best-fit model analysis. Note further that experimental (dashed lines) and calculated (solid lines) spectra are almost undistinguishable in Fig. 2 due to the good match between experimental and best-fit calculated data. Apparently, all spectra for the different compositions are quite similar, which means that the influence of boron on the electronic band structure of $B_xGa_{1-x}As$ alloys is rather small. We further note a small increase in the broadening of the $E_0{}'$, E_2, and $E_1{}'$ CP transitions, which we attribute to compositional fluctuations.

In Fig. 3, we present the second derivatives of the imaginary parts of the pseudodielectric functions of the GaN_yAs_{1-y}/GaAs samples including those for pure GaAs as well. Again, experimental (dashed lines) and calculated (solid lines) spectra are almost undistinguishable in Fig. 3 due to the good match between experimental and best-fit calculated data. The low-energy part of the pseudodielectric-function spectra ($0.75\ \text{eV} \leqslant E \leqslant 4.5\ \text{eV}$) of the GaN_yAs_{1-y}/GaAs samples is presented in Refs. 17 and 18 including a discussion of the CP's E_0, E_1, and $E_1+\Delta_1$. The assignment of the structures in Fig. 3 to different CP transitions is the same as for the $B_xGa_{1-x}As$ layers. We note that all CP structures of GaN_yAs_{1-y}, in comparison to $B_xGa_{1-x}As$ (see Fig. 2), are much more rapidly broadened with increasing nitrogen incorporation. This indicates that

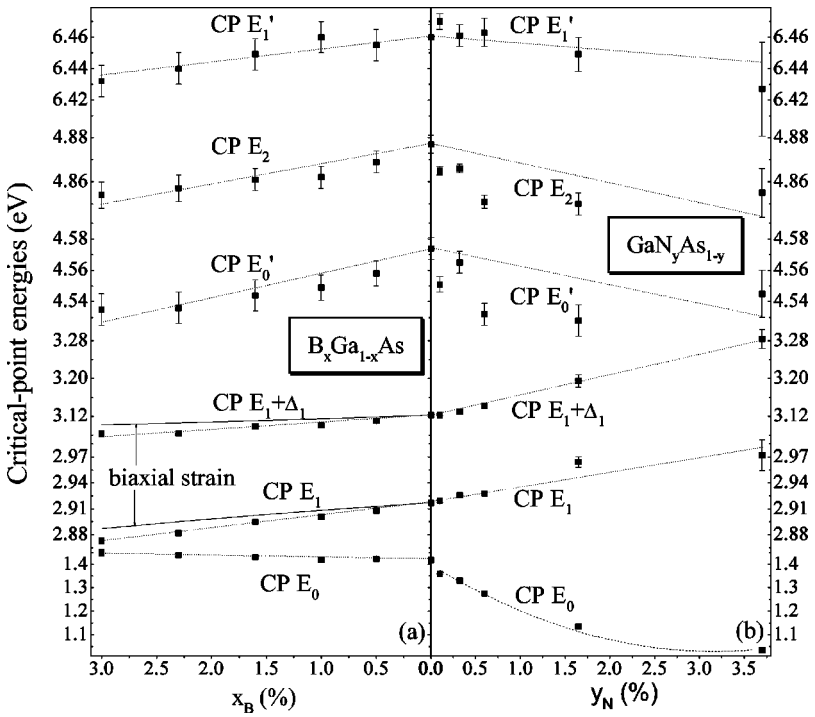

FIG. 4. Dependence of the E_0, E_1, $E_1+\Delta_1$, E_0', E_2, and E_1' CP-transition energies of $B_xGa_{1-x}As$ (a) and GaN_yAs_{1-y} (b) on the boron and nitrogen incorporation, respectively. The dotted lines are fits to the CP-transition energies. The solid lines correspond to the strain-induced shift of E_1, and $E_1+\Delta_1$ with x, and the dashed line is only shown as guide for the eye. The E_0, E_1, and $E_1+\Delta_1$ energies of GaN_yAs_{1-y} are reproduced from Refs. 17 and 18.

the effects of compositional fluctuations and clustering are much more pronounced in the GaN_yAs_{1-y} compared to the $B_xGa_{1-x}As$ material system.

The energies of the direct CP transitions of $B_xGa_{1-x}As$ and GaN_yAs_{1-y} resulting from the best-fit model analysis are presented in Figs. 4(a) and 4(b), respectively. For $B_xGa_{1-x}As$, all CP-transition energies are slightly redshifted with increasing boron incorporation except for E_0, which increase slightly with increasing x. In order to describe the observed $E_{CP}(x)$ dependencies, we use the CP-transition energies of BAs (extracted from the calculation of Hart and Zunger)[5] together with the corresponding CP energies of GaAs (extracted from our data analysis) for a linear interpolation of all CP-transition energies. The corresponding $E^{CP}(x)$ dependencies are then approximated by the following expression (dotted lines in Fig. 4):

$$E^{CP}(x)=E^{CP}(0)+[E^{CP}(1)-E^{CP}(0)]x-bx(1-x). \tag{3}$$

The direct CP transitions of GaN_yAs_{1-y} [see Fig. 4(b)] are described by Eq. (3) as well.

1. E_0 transitions

To begin with the band-gap energies of $B_xGa_{1-x}As$, we note first that BAs is an indirect semiconductor with Γ_{8v}-X_{6c} as the indirect band-gap transition.[5] However, for the B-composition range studied here, there are no experimental or theoretical hints for a direct to indirect crossover, and thus, our $B_xGa_{1-x}As$ ($0\leqslant x\leqslant 0.03$) layers should be direct semiconductors, which is confirmed by photoluminescence measurements.[13] For the lowest direct Γ-point transition energy of BAs (Γ_{8v}-Γ_{7c}), we use a value of 3.05 eV taken from Ref. 5 and obtain a bowing parameter of $b=(0.7\pm0.1)$ eV. This value is within the same region as the reported values of Geisz *et al.* ($b=2$ eV, transmission and PL),[4] Gottschalch *et al.* ($b=1.7$ eV, PL),[13] and Hart *et al.* ($b=3.5$ eV, calculation).[5] Note, however, that no reliable experimental data for the Γ_{8v}-Γ_{7c} transition of BAs are available in the literature. Existing theoretical values vary significantly (3.05–4.23 eV).[5,8] Thus, depending on the chosen theoretical value for the Γ_{8v}-Γ_{7c} transition of BAs, the obtained bowing parameters vary as well. Alternatively, the band-gap energies obtained in this work can also be well approximated by a straight line with a slope of $dE_0/dx=1.1$ eV.

A discussion of the band-gap energies GaN_yAs_{1-y} has already been included in Ref. 18. We find a strong redshift of the band-gap energy with increasing y, which has been obtained by many authors,[1] and theoretically described using different models.[29–32] The $E_0(y)$ dependence cannot be described using a composition-independent bowing parameter,[14] and the dashed line in Fig. 4 is only shown to guide the eye. Comparing the behavior of the band-gap energies of GaN_yAs_{1-y} to the $B_xGa_{1-x}As$ system, one clearly sees the different influences of boron and nitrogen on the bandstructure of GaAs. The physical origin of this is discussed in Sec. III C.

2. E_1 and $E_1+\Delta_1$ transitions

For the E_1 and $E_1+\Delta_1$ transitions of $B_xGa_{1-x}As$, we are not aware of the corresponding CP energies of BAs. Thus, the dotted lines in Fig. 4 are only linear approximations to the $E_1(x)$ and $(E_1+\Delta_1)(x)$ dependencies with linear increases of $dE_1/dx=(-1.5\pm0.1)$ eV and $d(E_1+\Delta_1)/dx=(-1.3\pm0.2)$ eV, respectively. The two solid lines depict the influence of biaxial, tensile strain on the two transition energies, which we have calculated using deformation-potential theory and the corresponding deformation poten-

tials of GaAs.[33] The strain-induced redshift of both CP's indicates that, depending on the exact value of the E_1 and $E_1+\Delta_1$ transition energies of BAs, the observed redshift of the E_1 and $E_1+\Delta_1$ CP energies in $B_xGa_{1-x}As$ should be mainly strain induced.

A discussion of the E_1 and $E_1+\Delta_1$ transition energies of GaN_yAs_{1-y} has already been included in Ref. 17. The observed blueshift of the E_1 and $E_1+\Delta_1$ CP energies with increasing nitrogen content has been reported by different groups.[17,34–36] In Ref. 17, we explained the blueshift of the E_1 transition energies with increasing nitrogen content as the sum of the effects of linear interpolation between the corresponding values of GaAs and cubic GaN and biaxial, tensile strain. The dotted lines in Fig. 4 have been obtained by fitting Eq. (3) to the $E_1(y)$ and $E_1+\Delta_1(y)$ dependencies of GaN_yAs_{1-y}. For the values of the binary end compounds, we used the corresponding values for GaAs ($y=0$) from the present work and the values for cubic GaN ($y=1$) from the literature [$E_1(1)=7.24$ eV experimentally determined in Ref. 37 and $E_1+\Delta_1(1)=7.27$ eV by addition of the spin-orbit splitting of $\Delta_1\cong 30$ meV calculated in Ref. 38]. As a result, we obtain (2.8 ± 0.2) eV and (-0.1 ± 0.1) eV for the bowing parameters of the CP's E_1 and $E_1+\Delta_1$, respectively. In Ref. 35, a bowing parameter of the E_1 transition of 1.5 eV was obtained.

3. E_0', E_2, and E_1' transitions

For application of Eq. (3) to the $E_0'(x)$, $E_2(x)$, and $E_1'(x)$ dependencies of $B_xGa_{1-x}As$, we take the corresponding calculated transition energies of BAs from Ref. 5 ($E_0':\Gamma_{6c}-\Gamma_{8v}=4.57$ eV, $E_2:x_{6c}-X_{6v}=5.34$ eV, $E_1':L_{4,5c}-L_{4,5v}=6.55$ eV), and obtain (1.6 ± 0.2) eV, (1.4 ± 0.1) eV, and (0.9 ± 0.1) eV, respectively, for the corresponding bowing parameters. Note that experimental data for the E_0', E_2, and E_1' transition energies of BAs are not available. Thus, the obtained bowing parameters depend on the chosen theoretical values as well, which vary significantly.[5,7]

The E_0', E_2, and E_1' transition energies of GaN_yAs_{1-y} show a similar dependence as the corresponding values in the $B_xGa_{1-x}As$ system. For application of Eq. (3), we use the transition energies of GaAs ($y=0$) from the present work and the values for cubic GaN ($y=1$) from the literature [$E_2(1)=7.57$ eV experimentally determined in Ref. 37, $E_0'(1)=10.6$ eV and $E_1'(1)=10.2$ eV calculated in Ref. 39]. As a result, we obtain $b=(7.4\pm0.5)$ eV, (3.7 ± 0.3) eV, and (5.7 ± 0.3) eV for the bowing parameters of the CP's E_0', E_2, and E_1', respectively. The $E_0'(y)$ and $E_2(y)$ dependencies deviate slightly from the applied approximation [Eq. (3)], which could be strain induced. Slightly decreasing or approximately constant E_0' and E_2 CP energies of GaN_yAs_{1-y} have already been found by Hung *et al.*[34] and Matsumoto *et al.*[35] In Ref. 35, a bowing parameter of the E_2 transition of 4.5 eV was obtained. For the CP E_1', we are not aware of an existing literature report.

To summarize Sec. III A, one could say that the obtained $E^{CP}(x)$ dependencies of $B_xGa_{1-x}As$ can be described by small bowing parameters. This indicates that the influence of boron on the band structure of $B_xGa_{1-x}As$ alloys is rather small. For GaN_yAs_{1-y} alloys, we obtain, in contrast to $B_xGa_{1-x}As$, a large redshift of the E_0 transition energies described by a large and composition-dependent bowing parameter. This shows the large influence of N on the band structure of GaN_yAs_{1-y}. All other CP transitions of GaN_yAs_{1-y} can be described by relatively small bowing parameters indicating that the band structure modification due to N should mainly occur at the conduction-band minimum at the Γ point of the BZ (the valence-band maximum is ruled out according to theoretical calculations).[29,30]

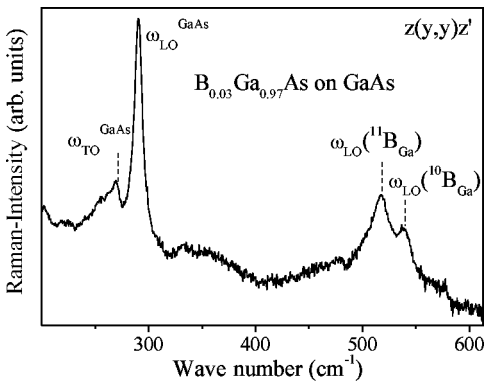

FIG. 5. Raman spectrum of a $B_{0.03}Ga_{0.97}As$/GaAs sample recorded at room temperature in the backscattering configuration.

B. BAs-like and GaN-like vibrations

The first observation of localized vibration modes (LVM) due to B_{Ga} isoelectronic substitutions in boron doped GaAs substrates was reported by Newman *et al.* using IR transmission at 77 K.[40] The authors found two lines at 517 and 540 cm^{-1} ($T=77$ K) caused by the incorporation of the stable isotopes ^{11}B and ^{10}B on Ga-lattice sites.[40] Boron has two stable isotopes with natural abundances of 0.8 (^{11}B) and 0.2 (^{10}B). Additionally, Newman *et al.* found two lines at 601 and 628 cm-1, which, according to subsequent reports, were caused by LVM's due to B_{As} isoelectronic substitutions.[41,42]

In Fig. 5, we present a Raman spectrum of a $B_{0.03}Ga_{0.97}As$/GaAs sample recorded in the backscattering configuration. The structure between 260 and 300 cm^{-1} is due to the TO and LO phonons of the GaAs sublattice of $B_xGa_{1-x}As$ (GaAs-like phonons) labeled $\omega_{TO}^{GaAs}/\omega_{LO}^{GaAs}$ in Fig. 5, and not to be mixed with the corresponding TO and LO phonons of the GaAs substrate/buffer layer. Note that the GaAs-like TO phonon is actually forbidden in the applied scattering configuration, but could be activated for instance, due to alloy disorder and/or deviation from the perfect $z(x,y)z'$ scattering condition. However, we did not obtain a significant increase of the TO/LO-intensity ratio with increasing boron incorporation. Besides the GaAs-like phonons, we detect a strong double structure between 510 and 540 cm^{-1}, which we attribute to the BAs-like LO phonons. This assignment follows the detection of the LVM of ^{11}B and ^{10}B in GaAs:B at 517 and 540 cm^{-1}, respectively,[40] and calculations of the LVM frequencies us-

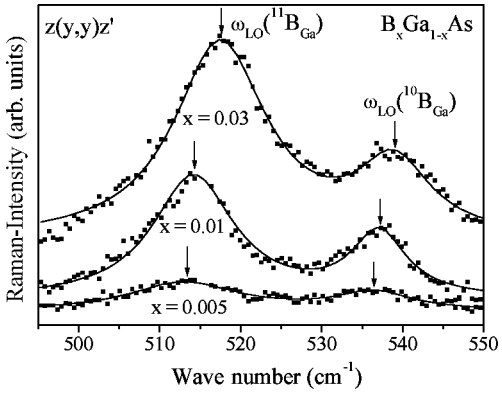

FIG. 6. Raman spectrum of three $B_xGa_{1-x}As/GaAs$ samples ($x=0.005$, 0.01, and 0.03) recorded at room temperature in the backscattering configuration. The solid lines refer to Lorentzian fits to the experimental data (symbols).

ing a linear diatomic-chain model,[43] which result in $\omega(^{11}B_{Ga})=523$ cm^{-1} and $\omega(^{10}B_{Ga})=546$ cm^{-1}. We did not observe a structure due to a B-Ga vibration (B on As lattice site) in our Raman spectra.

In Fig. 6, we show three (typical) Raman spectra of $B_xGa_{1-x}As/GaAs$ samples in the vicinity of the BAs-like phonon region. The solid lines refer to Lorentzian fits to the experimental data (symbols). Apparently, the intensity of the Raman scattering lines due to BAs-like phonons increases with increasing boron content. The $^{11}BAs/^{10}BAs$ LO-mode scattering-intensity ratio scatters between 2.5 and 4 and is thus close to the ratio of the natural isotope abundancies, which is $^{11}B/^{10}B=4/1$. Deviations from the ideal 4/1 ratio may arise from the existence of additional scattering due to disorder-activated GaAs-like two-phonon mode excitation in the BGaAs layers. In addition, we observe a blueshift of both phonon frequencies with increasing *x*, which is discussed below.

The mode frequencies of the ^{11}BAs-like and ^{10}BAs-like phonons resulting from the Lorentzian-line-shape analysis are shown in Fig. 7. The dotted lines are linear fits to the data points, whereas the solid lines depict the effect of linear interpolation between the phonon-mode frequencies of the binary end compounds. The latter has been calculated using the LO-phonon frequency of cubic BAs ($\omega_{LO}=714$ cm^{-1})[44] (no splitting between the ^{11}BAs and ^{10}BAs phonons has been observed in Ref. 44) and the extrapolated values for $x=0$ taken from this work. For both phonon modes, the actual linear increases [$d\omega^{11BAs}/d\omega=(169\pm10)$ cm^{-1}, $d\omega^{10BAs}d\omega=(97\pm5)$ cm^{-1}] are smaller than the alloy-induced blueshift with *x*, which may have been caused by the effect of biaxial, tensile strain. Because we are not aware of phonon-deformation potentials of the BAs phonon, we cannot calculate the effect of strain on the mode frequencies. The difference between the two linear increases could be due to different anharmonic phonon interactions (Isotopic effects on phonon frequencies and their temperature dependence have been discussed in Ref. 45), strain effects or the coupling of the BAs phonons with the GaAs phonon. At this point, the first-principles calculations would be helpful in order to clarify the orign of the observed isotopic differences. However, this is beyond the scope of the current paper.

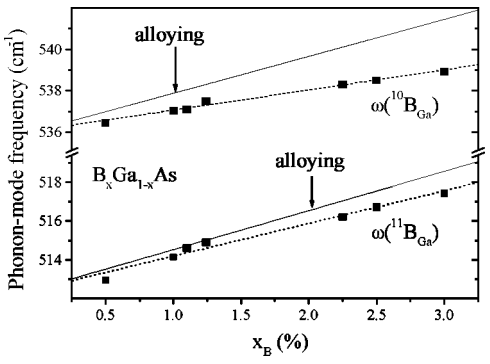

FIG. 7. Mode frequencies of the ^{11}BAs-like and ^{10}BAs-like phonons in $B_xGa_{1-x}As$ resulting from the Lorentzian-line-shape analysis. The dotted lines are linear fits to the data points, whereas the solid lines depict the effect of linear interpolation between the phonon-mode frequencies of the binary end compounds.

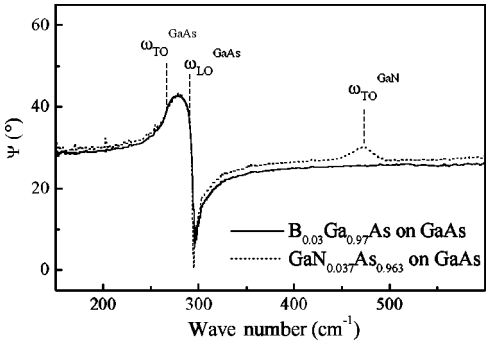

FIG. 8. Experimental Ψ spectra of a $GaN_{0.037}As_{0.963}/GaAs$ (dotted line, reproduced from Ref. 18) and a $B_{0.03}Ga_{0.97}As/GaAs$ (solid line) sample.

Beside Raman scattering, we also used infrared (IR) spectroscopy, such as IR transmission and IR ellipsometry for investigation of the phonon properties of $B_xGa_{1-x}As$ and GaN_yAs_{1-y} alloys. In the latter, we observed, in addition to the GaAs-like phonon, a GaN-like phonon at ~ 470 cm^{-1} using IR ellipsometry (see Ref. 18 for details). This is shown in Fig. 8 (dotted line) for a $GaN_{0.037}As_{0.963}$ layer as an example. On the other hand, there is no structure due to a BAs-like phonon in the spectrum of the $B_{0.03}Ga_{0.97}As/GaAs$ sample (solid line). From a simulation of the corresponding Ψ spectrum including one oscillator term for the BAs mode, we can estimate that the oscillator strength or polarity of the BAs-like phonon [$f=(\omega_{LO}-\omega_{TO})/\omega_{TO}$] is at least ten times smaller than the oscillator strength of the GaN-like phonon measured at a GaN_yAs_{1-y} layer with comparable thickness and composition.

We also performed IR transmission experiments but could not detect the BAs-like phonon as well. Note that Newman *et al.* did detect a LVM of B in GaAs using IR transmission spectroscopy at 77 K.[40] However, the experimental situation is different: Newman *et al.* used boron doped GaAs substrates, where, compared to our thin $B_xGa_{1-x}As$ layers

(thickness ~400 nm), the absorption due to the LVM of B in GaAs is drastically enhanced. On the other hand, our $B_xGa_{1-x}As$ and GaN_yAs_{1-y} layers have approximately the same thickness, are both deposited on GaAs substrates, and are therefore comparable. The physical origin of the different behavior of the BAs-like and the GaN-like phonon is discussed in the following section.

C. Ionicities of the B-As and Ga-N bonds

As shown in the last sections incorporation of boron and nitrogen in GaAs results in fundamentally different electronic and vibronic properties. At the first view, this might be surprising having in mind that both elements are relatively small with corresponding covalent radii of 0.85 Å (B) and 0.72 Å (N).[46] However, B and N are incorporated in different sublattices of the GaAs host crystal. Let us first consider the electronegativity values (EV) of the group-III and group-V elements. The elements boron, gallium, nitrogen, and arsenic have eV's of 2.01, 1.82, 3.07, and 2.20, respectively.[46] The differences may be understood by the following trends within the periodic table of the elements (PTE): (1) in each column of the PTE, the eV's decrease from the top to the bottom due to increased screening of the nucleus charge; (2) in each row of the PTE, the eV's decrease from the right to the left due to decreasing number of electrons in the outermost shell. These trends may also help to understand the ionicities of the B-As and Ga-N bonds, which amount to 0.002 and 0.5 on the Phillips scale, respectively.[47,48] This means that the B-As bond is almost purely covalent, whereas the Ga-N bond has a large ionic contribution. This is confirmed by recent calculations of Hart and Zunger.[5] The authors have pointed out that the bonding in BAs is much more covalent than in the rest of the group-III-As family, and that the band structure of BAs is more reminiscent of silicon than most other III-V compounds.

Several years ago, deep impurity levels caused by nitrogen in N-doped GaP (Ref. 49) and GaAs (Ref. 50) were detected by PL and transmission measurements. Local strain fields around the N atom and the large ionicity of the Ga-N bonds have been discussed to cause a strong short ranging potential giving rise to the observed impurity levels.[51–53] Because of the difference in ionicities, we can thus conclude that the short ranging potential is much weaker in GaBAs compared to GaNAs. Likewise, deep impurity levels caused by boron in B-doped GaAs have not been observed. On the other hand, Zunger and co-workers have pointed out that the unusually large and composition-dependent band-gap bowing in GaNAs can be traced back to the existence of a deep N-related level in the impurity limit.[54,55] In view of this the small bowing coefficient in GaBAs can be understood.

Considering the phonon properties, the low ionicity of the B-As bond results in a correspondingly small dipole moment. This explains that the observed oscillator strength of the Ga-N phonon (resulting from IR ellipsometry) is at least ten times larger than the oscillator strength of the B-As phonon.

IV. SUMMARY

We reported on spectroscopic ellipsometry and Raman-spectroscopy investigations of $B_xGa_{1-x}As$ ($0 \leqslant x \leqslant 0.03$) and GaN_yAs_{1-y} ($0 \leqslant y \leqslant 0.037$) alloys. For $B_xGa_{1-x}As$, we obtained only a small bowing coefficient of the $E_g(x)$ dependence in contrast to the giant redshift of the GaN_yAs_{1-y} band-gap energy with y. All higher lying interband-transition energies of $B_xGa_{1-x}As$ (E_1, $E_1+\Delta_1$, E_0', E_2, and E_1') are slightly redshifted with increasing boron concentration. A similar behavior is found for the CP's E_0', E_2, and E_1' in GaN_yAs_{1-y}. In $B_xGa_{1-x}As$, we observe, as in GaN_yAs_{1-y}, a two-mode phonon behavior. However, the oscillator strength of the B-As phonon is at least one order of magnitude smaller than the oscillator strength of the Ga-N phonon. All results are explained using a simple model that takes into account the different nature of the chemical bonds in both alloy types.

ACKNOWLEDGMENTS

This work is supported by Deutsche Forschungsgemeinschaft under Grant No. Go 629/4-2, by BMBF, and by the National Science Foundation under Contract No. DMI-9901510. Additionally, we wish to thank U. Teschner for experimental support.

*Electronic address: leibiger@rz.uni-leipzig.de; URL: http://www.uni-leipzig.de/~hlp/ellipsometrie/

[1] I.A. Buyanova, W.M. Chen, and B. Monemar, MRS Internet J. Nitride Semicond. Res. **6**, 1 (2001).
[2] M. Weyers, M. Sato, and H. Ando, Jpn. J. Appl. Phys., Part 2 **31**, L853 (1992).
[3] M. Kondow, S. Nakatsuka, T. Kitatani, Y. Yazawa, and M. Okai, Jpn. J. Appl. Phys., Part 1 **35**, 5711 (1996).
[4] J.F. Geisz, D.J. Friedman, J.M. Olson, S.R. Kurtz, R.C. Reedy, A.B. Swartzlander, B.M. Keyes, and A.G. Norman, Appl. Phys. Lett. **76**, 1443 (2000).
[5] G.L. Hart and A. Zunger, Phys. Rev. B **62**, 13 522 (2000).
[6] J.A. Perri, S. LaPlaca, and B. Post, Acta Crystallogr. **11**, 310 (1958).
[7] M.P. Surh, S.G. Louie, and M.L. Cohen, Phys. Rev. B **43**, 9126 (1991).
[8] C. Prassad and M. Sahay, Phys. Status Solidi B **154**, 201 (1989).
[9] S.M. Ku, J. Electrochem. Soc. **113**, 813 (1966).
[10] T.L. Chu and A.E. Hyslop, J. Electrochem. Soc. **121**, 412 (1974).
[11] J.F. Geisz, D.J. Friedman, J.M. Olson, S.R. Kurtz, R.C. Reedy, A.B. Swartzlander, and A.G. Norman, J. Cryst. Growth **225**, 372 (2001).
[12] V.K. Gupta, M.W. Koch, N.J. Watkins, Y. Gao, and G.W. Wicks, J. Electron. Mater. **29**, 1387 (2000).
[13] V. Gottschalch, G. Leibiger, and G. Benndorf, J. Cryst. Growth **248**, 468 (2002).
[14] W.G. Bi and C.W. Tu, Appl. Phys. Lett. **70**, 1608 (1997).
[15] W.E. Hoke, P.J. Lemonias, D.G. Weir, and H.T. Hendriks, J. Vac. Sci. Technol. B **11**, 902 (1993).
[16] M.A. Tischler, P.M. Mooney, B.D. Parker, F. Cardone, and M.S. Goorsky, J. Appl. Phys. **71**, 984 (1992).

[17] G. Leibiger, V. Gottschalch, B. Rheinländer, J. Šik, and M. Schubert, Appl. Phys. Lett. **77**, 1650 (2000).
[18] G. Leibiger, V. Gottschalch, B. Rheinländer, J. Šik, and M. Schubert, J. Appl. Phys. **89**, 4927 (2001).
[19] J. Šik, M. Schubert, G. Leibiger, V. Gottschalch, G. Kirpal, and J. Humlıček, Appl. Phys. Lett. **76**, 2859 (2000).
[20] J. Šik, M. Schubert, G. Leibiger, V. Gottschalch, and G. Wagner, J. Appl. Phys. **89**, 294 (2001).
[21] R. M. Azzam and N. M. Bashara, *Ellipsometry and Polarized Light* (North-Holland, Amsterdam, 1999).
[22] D. E. Aspnes, in *Handbook of Optical Constants of Solids*, edited by E. D. Palik (Academic, New York, 1998), Vol. I, p. 89.
[23] C.W. Higginbotham, M. Cardona, and F. Pollack, Phys. Rev. **184**, 821 (1969).
[24] S. Adachi, Phys. Rev. B **35**, 7454 (1987).
[25] M. Schubert, J.A. Woollam, G. Leibiger, B. Rheinländer, I. Pietzonka, T. Saß, and V. Gottschalch, J. Appl. Phys. **86**, 2025 (1999).
[26] P.Y. Yu and M. Cardona, *Fundamentals of Semiconductors* (Springer, Berlin, 1996).
[27] D.E. Aspnes, C.G. Olson, and D.W. Lynch, Phys. Rev. B **12**, 2527 (1975).
[28] P. Lautenschlager, M. Garriga, S. Logothetidis, and M. Cardona, Phys. Rev. B **35**, 9174 (1987).
[29] P. Kent and A. Zunger, Phys. Rev. Lett. **86**, 2613 (2001).
[30] T. Matilla, S.-H. Wei, and A. Zunger, Phys. Rev. B **60**, R11 245 (1999).
[31] W. Shan, W. Walukiewicz, J.W. Ager III, E.E. Haller, J.F. Geisz, D.J. Friedmann, J.M. Olson, and S.R. Kurtz, Phys. Rev. Lett. **82**, 1221 (1999).
[32] Y. Zhang, A. Mascarenhas, H.p. Xin, and C.W. Tu, Phys. Rev. B **61**, 7479 (2000).
[33] M. Chandrasekhar and F.H. Pollak, Phys. Rev. B **15**, 2127 (1977).
[34] W.K. Hung, M.Y. Chern, Y.F. Chen, Z.L. Yang, and Y.S. Huang, Phys. Rev. B **62**, 13 028 (2000).
[35] S. Matsumoto, H. Yaguchi, S. Kashiwase, T. Hashimoto, S. Yoshida, D. Aoki, and K. Onabe, J. Cryst. Growth **221**, 481 (2000).
[36] J. Wagner, K. Köhler, P. Ganser, and N. Herres, Appl. Phys. Lett. **77**, 3592 (2000).
[37] A. Kasic, M. Schubert, T. Frey, U. Köhler, D.J. As, and C.M. Herzinger, Phys. Rev. B **65**, 184302 (2002).
[38] M. Cardona and N.E. Christensen, Solid State Commun. **116**, 421 (2000).
[39] K. Miwa and A. Fukumoto, Phys. Rev. B **48**, 7897 (1993).
[40] R.C. Newman, F. Thompson, M. Hyliands, and R.F. Peart, Solid State Commun. **10**, 505 (1972).
[41] J. Woodhead, R.C. Newman, I. Grant, D. Rumsby, and R.M. Ware, J. Phys. C **16**, 5523 (1983).
[42] D.N. Talwar, M. Vandevyver, K.K. Bajaj, and W.M. Theis, Phys. Rev. B **33**, 8525 (1986).
[43] G. Lucovski, M.H. Brodsky, and E. Burstein, Phys. Rev. B **2**, 3295 (1970).
[44] R.G. Greene, H. Luo, A.L. Ruoff, S.S. Trail, and F.J. DiSalvo, Jr., Phys. Rev. Lett. **73**, 2476 (1994).
[45] J. Serrano, M. Cardona, T. M. Ritter, B. A. Weinstein, A. Rubio, and C. T. Lin, Phys. Rev. B **66**, 245202 (2002).
[46] H.-J. Bautsch, J. Bohm, and I. Kleber, *Einführung in die Kristallographie* (Verl. Technik, Berlin, 1990).
[47] J.A. Van Vechten, Phys. Rev. **187**, 1007 (1969).
[48] J. C. Phillips, *Bonds and Bands in Semiconductors* (Academic, New York, 1973).
[49] D.G. Thomas and J.J. Hopfield, Phys. Rev. **150**, 680 (1966).
[50] D. J. Wolford, J. A. Bradley, K. Fry, and J. Thompson, in *Proceedings of the 17th International Conference on the Physics of Semiconductors*, edited by J. D. Chadi and W. A. Harrison (Springer, New York, 1984), p. 627.
[51] R.A. Faulkner, Phys. Rev. **175**, 991 (1968).
[52] J.W. Allen, J. Phys. C **1**, 1136 (1968).
[53] J.C. Phillips, Phys. Rev. Lett. **22**, 285 (1968).
[54] S.-H. Wei and A. Zunger, Phys. Rev. Lett. **76**, 664 (1996).
[55] L. Bellaiche, S.-H. Wei, and A. Zunger, Appl. Phys. Lett. **70**, 3558 (1997).